Supplementary Material to:
Gaussian Process Emulation to Accelerate Parameter Estimation in a Mechanical Model of the Left Ventricle: a Critical Step towards Clinical End-user Relevance

Umberto Noè[1,*], Alan Lazarus[2,*], Hao Gao[2], Vinny Davies[2,3], Benn Macdonald[2], Kenneth Mangion[4,5], Colin Berry[4,5], Xiaoyu Luo[2], and Dirk Husmeier[2,c]

[1]German Center for Neurodegenerative Diseases (DZNE), Bonn, Germany.
[2]School of Mathematics and Statistics, University of Glasgow, Glasgow, UK.
[3]School of Computing Science, University of Glasgow, Glasgow, UK.
[4]BHF Glasgow Cardiovascular Research Centre, University of Glasgow, Glasgow, UK.
[5]West of Scotland Heart and Lung Centre, Golden Jubilee National Hospital, Clydebank, UK.
[*]Authors contributed equally.
[c]Corresponding author: dirk.husmeier@glasgow.ac.uk

1 Convolved Multiple Output GP

In the biomechanical model, the outputs of the simulator correspond to measures of circumferential strains at different locations of the LV wall and the overall LV volume. It appears justified to assume an inherent process governing the strains of the LV, related to the underlying cardiomechanic pump cycle. Treating this as some latent process x we may assume the outputs to be explicitly dependent on this process:

$$\boldsymbol{y}_l(\cdot) = \boldsymbol{f}(x_l(\cdot)) + \epsilon(\cdot) \tag{1}$$

Under this framework, modelling of this latent process as a GP leads to a GP prior over the outputs of the system, since GP priors are closed under linear maps. Moreover, crosscovariance between the outputs is induced by the autocovariance of this underlying latent process, providing a dependency between the outputs of the simulator. Alvarez and Lawrence (2011) rely on this idea to introduce correlations between multiple outputs. Drawing on the idea of the linear model of corregionalization (eq. 1 with $f(\cdot)$ a finite linear map), they assume m independent underlying latent processes modelled using GPs, $x_j(\cdot)$, and postulate that the output can be represented as a convolution between a smoothing kernel $S_{d,j}(\cdot)$ and these latent functions, subject to additive i.i.d. Gaussian noise $\epsilon_d(\boldsymbol{q})$:

$$y_l(\boldsymbol{q}) = \sum_{j=1}^{M} \int_{\Theta} S_{l,j}(\boldsymbol{q} - \boldsymbol{z}) x_j(\boldsymbol{z}) d\boldsymbol{z} + \epsilon_d(\boldsymbol{q}) \tag{2}$$

where Θ is the design space of the emulator and M is the number of latent functions. The smoothing kernel, $S_{l,j}(\cdot)$ controls the influence of latent function x_j on output l, allowing unique measures of smoothness in all outputs. The convolution operator introduces more general mixing of the latent process than in the LMC and the resultant process is also a GP. Resultantly, they obtain covariances between the outputs:

$$\begin{aligned}\mathrm{Cov}(y_i(\boldsymbol{q}_1), y_k(\boldsymbol{q}_2)) = \sum_{j=1}^{M}\sum_{j'=1}^{M} \int_{\Theta} S_{i,j}(\boldsymbol{q}_1 - \boldsymbol{z}) \\ \int_{\Theta} S_{k,j'}(\boldsymbol{q}_2 - \boldsymbol{z}) \mathrm{Cov}(x_j(\boldsymbol{z}), x_{j'}(\boldsymbol{z})) d\boldsymbol{z}' d\boldsymbol{z} \\ + \mathrm{Cov}(\epsilon(\boldsymbol{q}_1), \epsilon(\boldsymbol{q}_2))\end{aligned} \tag{3}$$

which is simplified under the common assumption of mutually independent latent processes. Problematically, this method requires expensive estimation of parameters of both the convolution kernel and the kernel of the underlying latent process, culminating in the inference of parameters via the likelihood function:

$$p(\boldsymbol{y}|\boldsymbol{x}, \boldsymbol{q}) = \mathrm{N}(\boldsymbol{0}, \boldsymbol{\Omega} + \boldsymbol{\Sigma}) \tag{4}$$

where elements of $\boldsymbol{\Omega}$ provide covariances between outputs at different design points and Σ gives the (diagonal) covariance matrix of the additive noise from eq. 1. Evaluation of the likelihood is of the order $\mathcal{O}(M^3D^3)$ for M outputs with D measurements of each (D is the size of our design set). This incurs high computation cost, and the computations become infeasible if one wishes to use the full design. Moreover, one has to tune the number of latent processes, perhaps using some measure of the marginal likelihood.

The MSE in parameter estimates obtained via the method of Alvarez and Lawrence is provided in Figure 1. Here we see the increased error in our estimates

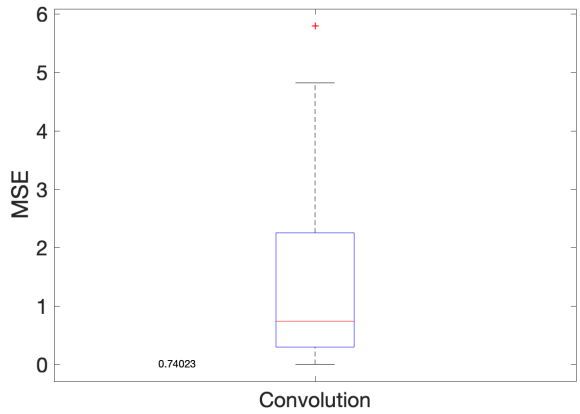

Figure 1: Results from parameter estimation using the multiple output method of Alvarez and Lawrence. MSE in parameter estimates obtained using a function space local GP with the method of Alvarez and Lawrence.

of the parameters compared with the method of Conti and O'Hagan. This may result from a lack of training of the latent process of the GP.

2 Discussion on the global optimization algorithm choice

The Global Search algorithm was shown to effectively search for the global optimum even in high-dimensional spaces due to the construction of several basins of attractions, which lead to a more thorough search over the whole domain (an experimental evaluation of the effectiveness of the algorithm is discussed in Pál et al. (2012)). The basins of attraction help excluding the domain regions which were previously searched by a local solver and emphasize exploration of new domain areas. This should be contrasted to standard multi-start algorithms which scatter random starting points and blindly run multiple local solvers. The drawback of this latter approach is that the random initial points could be close to each other, hence increasing the chance of finding a local minimum. This possibility could be alleviated by resorting to space-filling designs like Sobol sequences. However, rather than running a local solver from each point in the space-filling design, the construction of basins of attraction has the advantage of substantially reducing the number of initial points from which to start a local solver.

Before summarizing the algorithm, we define the concept of a *basin of attraction*. Consider running a local solver from a given starting point $\boldsymbol{q}_0$, ending up at point of local minimum $\hat{\boldsymbol{q}}$. The *basin of attraction* associated to that local minimum is defined as the sphere[1] centred at $\hat{\boldsymbol{q}}$ with radius $\|\boldsymbol{q}_0 - \hat{\boldsymbol{q}}\|$. All starting points falling inside the sphere are assumed to lead to the same local minimum $\hat{\boldsymbol{q}}$; hence no local solver is run from those starting points and they are discarded.

In simple terms, stage one of the Global Search algorithm scatters starting points in the input space and scores them from best to worst by evaluating their objective function value and constraint violations. Then, an interior-point local solver (Byrd et al., 2000) is run from each trial point, starting from the one that was scored best (lowest function value), and excluding points that fall into the basins of attraction of previously found minima. When all the stage one points have been analyzed, stage two generates more random points and the same procedure is run for a second time.

3 Further details on the simulated data

For a fixed LV geometry and parameter bounds $[q_1^L, q_1^U] \times \cdots \times [q_4^L, q_4^U]$, we generated $n = 10,000$ points $\boldsymbol{q}_1, \ldots, \boldsymbol{q}_n$ from a Sobol sequence and solved the PDE model using the finite elements method for each parameter vector to obtain the corresponding simulations $\mathbf{m}(\boldsymbol{q}_1), \ldots, \mathbf{m}(\boldsymbol{q}_n)$. The inputs and corresponding simulations together form the training set which is used to build the emulator. Then, we generated extra $n_{\text{test}} = 100$ parameters by extending the Sobol sequence and ran extra forward simulations for each of those, in order to obtain a test set. This ensures that the test data are different from the trainig data (to avoid bias) and that their corresponding parameter vectors uniformly cover the whole space (so as to be representative).

4 Circumferential strains

The end-diastolic volume and peak diastolic segmental circumferential strains were chosen for the measured data from the cardiac MR imaging data and the forward LV simulators, similar as in our previous study (Gao et al., 2017). The reasons of choosing circumferential strains are that (1) our previous study (Gao et al., 2014) has shown that the circumferential strains can be accurately estimated from cine images using a B-spline nonlinear registration approach compared to strain MRI, i.e. DENSE sequence (Displacement Encoding with Stimulated Echoes); (2) various studies (Augustine et al., 2013) have found that the longitudinal and radial strains estimated from cine MR images are poorer compared to the circumferential strain using feature-tracking approaches; (3) full 3-dimensional strain fields (circumferential, radial and longitudinal strains) could in principle be

[1] The spherical nature of the basins of attractions is a heuristic assumption of the algorithm.

acquired using MRI (Zhong et al., 2010), but are not routinely available in the clinic yet.

References

Alvarez, M. A. and Lawrence, N. D. (2011). Computationally efficient convolved multiple output gaussian processes. *Journal of Machine Learning Research*, 12:1459–1500.

Augustine, D., Lewandowski, A. J., Lazdam, M., Rai, A., Francis, J., Myerson, S., Noble, A., Becher, H., Neubauer, S., Petersen, S. E., and Leeson, P. (2013). Global and regional left ventricular myocardial deformation measures by magnetic resonance feature tracking in healthy volunteers: comparison with tagging and relevance of gender. *Journal of Cardiovascular Magnetic Resonance*, 15(1):8.

Byrd, R. H., Gilbert, J. C., and Nocedal, J. (2000). A trust region method based on interior point techniques for nonlinear programming. *Mathematical Programming*, 89(1):149–185.

Gao, H., Aderhold, A., Mangion, K., Luo, X., Husmeier, D., and Berry, C. (2017). Changes and classification in myocardial contractile function in the left ventricle following acute myocardial infarction. *Journal of The Royal Society Interface*, 14(132):20170203.

Gao, H., Allan, A., McComb, C., Luo, X., and Berry, C. (2014). Left ventricular strain and its pattern estimated from cine cmr and validation with dense. *Physics in Medicine & Biology*, 59(13):3637.

Pál, L., Csendes, T., Markót, M. C., and Neumaier, A. (2012). Black box optimization benchmarking of the global method. *Evolutionary Computation*, 20(4):609–639.

Zhong, X., Spottiswoode, B. S., Meyer, C. H., Kramer, C. M., and Epstein, F. H. (2010). Imaging three-dimensional myocardial mechanics using navigator-gated volumetric spiral cine dense mri. *Magnetic resonance in medicine*, 64(4):1089–1097.